Vibrational bands of luminescent zinc(II)-octaethyl-porphyrin using a polarization-sensitive 'microscopic' multiplex CARS technique

ARTICLE *in* JOURNAL OF RAMAN SPECTROSCOPY · JUNE 2001

Impact Factor: 2.67 · DOI: 10.1002/jrs.737

4 AUTHORS, INCLUDING:

Cees Otto
University of Twente
231 PUBLICATIONS **5,255** CITATIONS
SEE PROFILE

Sergei G Kruglik
Pierre and Marie Curie University - Paris 6
99 PUBLICATIONS **920** CITATIONS
SEE PROFILE

JOURNAL OF RAMAN SPECTROSCOPY
J. Raman Spectrosc. 2001; **32**: 495–501

JRS

Vibrational bands of luminescent zinc(II)-octaethylporphyrin using a polarization-sensitive 'microscopic' multiplex CARS technique

C. Otto,[1]* A. Voroshilov,[1] S. G. Kruglik[2] and J. Greve[1]

[1] University of Twente, Department of Applied Physics, Biophysical Technology, MESA$^+$-Research Institute, P.O. Box 217, 7500 AE Enschede, The Netherlands
[2] B. I. Stepanov Institute of Physics, National Academy of Sciences of Belarus, F. Skaryna Ave. 70, Minsk 220072, Belarus

Received 31 December 2000; Accepted 20 April 2001

Polarization-sensitive, multiplex coherent anti-Stokes Raman scattering (ps-MCARS) has been used to detect the vibrational bands of the highly luminescent zinc(II)-octaethylporphyrin (Zn-OEP). We show here that ps-MCARS can be used to measure the vibrational bands under resonant conditions. Polarization-sensitive CARS further helps to resolve composite and overlapping Raman bands on the basis of variations in vibrational symmetry. This paper also exemplifies the advantages of multiplex CARS (MCARS) spectroscopy carried out under tight focusing conditions as proposed earlier. We demonstrate that a 'microscopic' CARS focusing and collection system in combination with the multiplex technique allows a reduction in the amount of sample and a shortening of the measurement time. We analyse the relationship between the coherent vibrational phases and the symmetry of the different vibrational band of Zn-OEP skeletal modes. The values of the coherent vibrational phases are similar for vibrational bands with the same symmetry. Copyright © 2001 John Wiley & Sons, Ltd.

INTRODUCTION

Polarization-sensitive, multiplex coherent anti-Stokes Raman scattering (ps-MCARS) has been used to detect the vibrational bands of the highly luminescent zinc(II)-octaethylporphyrin (Zn-OEP). Alternative methods based on non-coherent Raman spectroscopy (SR) have yielded information on the totally symmetric vibrational (A_{1g}) modes. These modes can readily be observed when an excitation wavelength of 436[1,2] or 450 nm,[3] near the Soret absorption band, was used. The dispersion of Raman bands of cyclic tetrapyrroles (heme groups and other porphyrins) depends strongly on the excitation wavelength.[4–10] Changes in the excitation wavelength are accompanied by changes in the resonance Raman enhancement of modes, which depend on their symmetry. The vibrational bands with an A_{2g} or B_{1g}/B_{2g} symmetry require excitation wavelengths in closer proximity to the Q-absorption bands of Zn-OEP. In this range, however, the luminescent emission of Zn-OEP (quantum yield ~4%)[11] spectrally overlaps with the Raman scattering, rendering the latter unobservable. We show here that ps-MCARS can be used to measure the vibrational bands under resonant conditions. The interference with the luminescence is avoided because the coherent signal is shifted to the short-wavelength side of the excitation. Also, since the CARS signal is directed in space, it is also easy to minimize the collection of the luminescence. Polarization-sensitive CARS further helps to resolve composite and overlapping Raman bands on the basis of variations in vibrational symmetry.[12–15] Previously, this approach to other porphyrins and related compounds has been shown to be successful.[14,16–23]

Zn-OEP is an example of a porphyrin with nearly undistorted D_{4h} symmetry, which remains flat in non-coordinating solvents, such as toluene, and retains planarity upon the binding of a fifth ligand.[2] Hence one may expect that Zn-OEP is not subject to symmetry-lowering distortions[6,7] and allows a nice categorization in A_{1g}, A_{2g} or B_{1g}/B_{2g} modes. Therefore, this compound is useful for elucidating the relationship between the vibrational mode symmetry and the coherent vibrational phase that can be associated with these modes.

This paper also exemplifies the advantages of multiplex CARS (MCARS) spectroscopy carried out under tight focusing conditions as proposed earlier.[24] We demonstrate that a 'microscopic' CARS focusing and collection system in combination with the multiplex technique allows a reduction in the amount of sample and a shortening of the measurement time.

*Correspondence to: C. Otto, University of Twente, Department of Applied Physics, Biophysical Technology, MESA$^+$-Research Institute, P.O. Box 217, 7500 AE Enschede, The Netherlands.
E-mail: c.otto@tn.utwente.ul

DOI: 10.1002/jrs.737

JRS

EXPERIMENTAL

Instrumentation

The CARS spectrometer consisted of a mode-locked Nd: YLF laser (Coherent Antares 76), which is frequency-doubled to 527 nm using LBO. The laser output was used to pump synchronously two cavity-dumped dye lasers (Coherent 700). One dye laser contained Rhodamine 6G (R6G) as the active medium and the other contained DCM. The R6G dye laser was operating in a narrow-band mode, using a triple birefringent filter to select the wavelength between 560 and 615 nm. The DCM dye laser was converted to broad-band mode by removing the birefringent filter from the cavity. A broad spectrum was generated with a width of 12 nm around 634 nm. Polarizing optics were present in each of the two beams for the purpose of polarization-sensitive CARS. Figure 1 shows a detail of the sample space.

The sample was passed through a square-shaped capillary (borosilicate glass, inner thickness 200 μm, wall thickness 50 μm) by means of a peristaltic pump (~10 μl s^{-1}). The pump (λ_1) and Stokes ($\Delta\lambda_2$) beams were superimposed using a 50:50 beamsplitter in a non-critical phase-matching scheme.

A pair of microscope objectives (40×, $NA = 0.4$, both Olympus), arranged head-to-head, was used to focus the incident radiation on the sample and to collect the CARS scattered continuum. The scattered radiation was spectrally filtered with a holographic notch filter (590 nm, Kaiser Optics). The detection system consisted of a single-stage $f/5$ polychromator (HR 320, 1800 lines mm^{-1}, Jobin Yvon) and a liquid nitrogen-cooled CCD camera (512 × 512, 22 μm per pixel, Princeton Instruments). The entrance slit of the polychromator was adjusted to 30 μm. This resulted in a spectral resolution of ~3.8 cm^{-1} and a spectral coverage from 1100 to 1700 cm^{-1}.

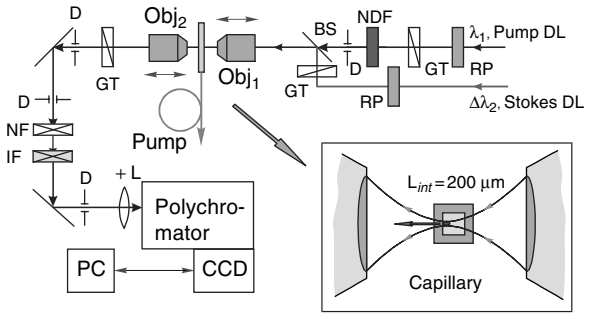

Figure 1. Optical layout of the microscopic sample compartment and the detection stage of the picosecond CARS spectrometer. BS = beamsplitter; RP = retardation plate; GT = Glan–Taylor polarizer; D = diaphragm; ±L = positive/negative lens; NF = notch filter; IF = interference filter; NDF = neutral density circular filter; CCD = charge-coupled device detector; PC = personal computer. The sample solution is passed through a square capillary positioned between two microscope objectives (Obj1, Obj2), with superimposed focal volumes (see the inset).

The polarization-sensitive CARS spectra were obtained with the polarization of the incident Stokes' beam ($\mathbf{e}_2$) adjusted in a vertical plane. This beam made an angle of 60° with the pump beam ($\mathbf{e}_1$). The polarization purity for the whole microscope stage was checked and found to be better than 10^{-4} for linearly polarized light. Polarised MCARS spectra were obtained for seven different orientations of the analyser ($\mathbf{e}_A$). The angle between $\mathbf{e}_A$ and $\mathbf{e}_1$ varied between 90° and 0° in steps of 15°. Simultaneous fitting of the seven spectra to the CARS susceptibility allowed a very accurate determination of the components $\chi^{(3)}_{1111}$ and $\chi^{(3)}_{1221}$ in the overall susceptibility $\chi^{(3)} = \chi^{(3)NR} + \chi^{(3)R}$.

Fitting of the resonant CARS spectra

The fitting of the CARS spectra has been explained elsewhere[22] and is briefly summarized as follows. The dispersion of the intensity of CARS signal can be written as

$$I_{CARS}(\omega_3) \propto \left| p^{NR}\chi^{NR} + p^{E}\chi^{E}\exp(i\Theta^{E}) + \sum_t p_t^{R}\frac{A_t^{R}\exp(i\Theta_t^{R})}{\Omega_t - (\omega_1 - \omega_2) - i\Gamma_t/2}\right|^2 \quad (1)$$

here Ω_t, Γ_t, A_t^R and Θ_t^R are, respectively, the frequency, width, amplitude and phase of the tth Raman transition. The coherent phases Θ_t^R are only considered for the vibrations of the sample molecules, whose susceptibility $\chi^{(3)R}$ is resonantly enhanced. The complexity of the electronic susceptibility is introduced as $\chi^{(3)E} = \chi^{(3)E}\exp(i\Theta^E)$. The summation in Eqn. (1) runs over all t vibrations with configuration factors:

$$p^{NR,E,R} = [(1 - \rho^{NR,E,R})(\mathbf{e}_A^*\mathbf{e}_1)(\mathbf{e}_1\mathbf{e}_2^*) + \rho^{NR,E,R}(\mathbf{e}_1^*\mathbf{e}_2^*)], \quad (2)$$

where unit vector $\mathbf{e}_A$ denotes the transmission plane of the polarization analyser through which the CARS field is viewed, and the coherent depolarization ratios are defined as

$$p^{NR,E,R} = \chi^{(3)NR,E,R}_{1221} \Big/ \chi^{(3)NR,E,R}_{1111} \quad (3)$$

with the additional relation, $\rho^{NR} = 1/3$, which is a result from optically transparency and isotropy of the solvent. The superscripts NR, E and R in Eqns (1)–(3) denote the terms arising from the non-resonant background, purely electronic and vibrationally resonant parts of the overall susceptibility, respectively.

The accuracy with which the CARS spectra can be fitted can be increased if not only the dispersion of the pure components $\chi^{(3)}_{1111}$ and $\chi^{(3)}_{1221}$ are considered, but also of their linear combinations. Using different analyser orientations different linear combinations are obtained. In particular, for analyser settings at 90, 60, 30 and 0° and an angle

of 60° between the polarization of the pump and the Stokes beam the following combinations are observed: $\chi^{(3)}_{1221}$, $(\chi^{(3)}_{1111} - 3\chi^{(3)}_{1221})$, $(\chi^{(3)}_{1111} - \chi^{(3)}_{1221})$ and $\chi^{(3)}_{1111}$.

MATERIALS

Zinc(II)-octaethylporphyrin was used without further purification. All experiments were carried out with a solution of Zn-OEP in toluene (~0.5 mM) at ambient temperature. In Fig. 2 the UV–visible absorption spectrum of Zn-OEP is shown together with the excitation wavelength arrangement as used in the MCARS experiments. The pump wavelength λ_1 (580.1 nm) was chosen preresonantly to the Q_{00} band of Zn-OEP ground-state absorption at 570 nm. The Stokes dye laser was optimized to generate an ~11.5 nm broad continuum $\Delta\lambda_2$ centred at 634 nm. A vibrational range of ~600 cm^{-1} could thus be covered. The anti-Stokes continuum $\Delta\omega_{CARS} = 2\omega_1 - \Delta\omega_2$ is in resonance with the Q_{01} band of Zn-OEP absorption. The dominant contribution to the enhancement of the susceptibility $\chi^{(3)R}$ was attained through the electronic resonances at $\omega_{CARS} \approx \Omega_{Q01}$ and $\omega_1 \approx \Omega_{Q00}$.

RESULTS AND DISCUSSION

Polarized MCARS spectra of Zn-OEP

Figure 3 shows two sets of polarized MCARS spectra of the neat solvent (toluene) and of Zn-OEP in solution. Only four of the seven spectra belonging to each set are represented. The analyser settings corresponded to an angle of (a) 90, (b) 60, (c) 30 and (d) 0° with the polarization of the pump beam.

The major porphyrin bands are best seen in the background suppressed spectra in Fig. 3(b) (right panel). The estimate of their polarization character readily follows from comparison of the amplitude ratios of $\chi^{(3)}_{1111}$ and $\chi^{(3)}_{1221}$ spectra

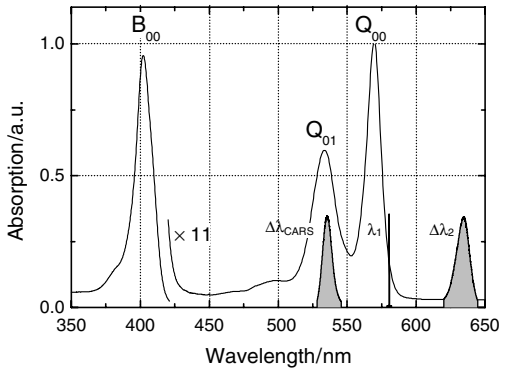

Figure 2. Optical absorption of Zn-OEP in solution (~0.5 mM in toluene) and MCARS excitation conditions. Absorption in the Q band range is magnified. Shaded areas display the broadband Stokes laser emission $\Delta\lambda_2$ (at right) and the non-resonant background profile $\Delta\lambda_{CARS}$ (at left).

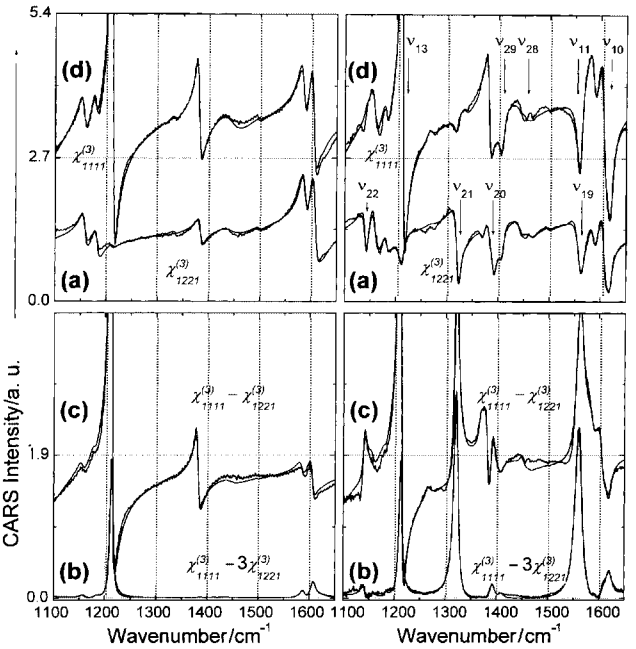

Figure 3. Left panels: polarized MCARS spectra of neat toluene (thin lines) showing the dispersion of sole $\chi^{(3)}_{1221}$ and $\chi^{(3)}_{1111}$ components [(a) and (d), respectively], and of their combinations $\chi^{(3)}_{1111} - 3\chi^{(3)}_{1221}$ and $\chi^{(3)}_{1111} - \chi^{(3)}_{1221}$ [(b) and (c), respectively]. Right panels: polarized MCARS spectra of Zn-OEP solution in toluene showing the dispersion of analogous susceptibility components. The lowest profiles in each panel (b) are the non-resonant background-free spectra. Experimental conditions: $\tau_{pulse} \approx 5$ ps; pump pulse energy = 0.5 nJ; Stokes pulse energy = 7.2 nJ; repetition rate = 3.8 MHz; accumulation time = 80 s. The spectra are normalized on the non-resonant background profile measured of the capillary material. Bold lines display the best simultaneous spectral fits with parameters listed in Table 1.

[profiles (d) and (a), respectively]. A very intense and highly polarized ($\rho^R \to 0$) band of toluene at ~1210 cm^{-1} and a pair of its depolarized ($\rho^R \to 0.75$) bands at ~1580–1600 cm^{-1} [Fig. 3(b), left panel] can be used as a convenient reference in qualitative assignments of Zn-OEP vibrational symmetries. The activity of antisymmetric (anomalously polarized) A_{2g} modes near 1141 (ν_{22}), 1320 (ν_{21}), 1391 (ν_{20}) and 1560 (ν_{19}) cm^{-1} is apparent [(a) in Fig. 3]; the presence of depolarized B_{1g}/B_{2g} modes is not so readily discernible. Except for a strong feature at ~1618 (ν_{10}) cm^{-1}, the depolarized porphyrin bands are obscured either by toluene bands (such as at 1210 cm^{-1}) or by anomalously polarized bands of porphyrin (such as at 1560 cm^{-1}).

The sign with which non-linear electric polarisations $\mathbf{P}^{(3)R}$ and $\mathbf{P}^{(3)NR}$ interfere depends on the relative signs of their projections on the analyser transmission plane and on the coherent vibrational phase. As one can see from Fig. 3 (left panel), all the bands of the optically transparent toluene (zero vibrational phase) show a positive dispersive

lineshape, independent of the analyser orientation. The lineshape displayed by the strongest porphyrin vibrations at 1150, 1315 and 1560 cm^{-1} is nearly Lorentzian and it changes from negative to positive on going from spectrum (a) to spectrum (c) in Fig. 3 (right panel). Such behaviour supports our tentative assignments of these bands to antisymmetric A_{2g} porphyrin modes. Also, the coherent vibrational phases for these modes appear to be similar. The exact values of coherent depolarization ratios and vibrational phases can only be established from the simultaneous lineshape analysis of the CARS spectra.

Vibrational assignment in Zn-OEP

In Table 1 the results of the fit are presented together with the symmetry assignment of the vibrational bands of Zn-OEP. This assignment is guided by the value of the coherent depolarization ratios. The assignment is consistent with (i) a set of assignments reported for Zn-OEP modes when the porphyrin is excited near the Soret band,[2,3] (ii) a normal-coordinate analysis in modified and substituted Ni-OEPs[5,9] and (iii) other CARS experimental data on various metallo-octaethylporphyrins.[7–10,17–19,21]

Resonance Raman studies of Zn-OEP, with an excitation wavelength of 436[2] or 450 nm,[3] have provided detailed information on totally symmetric A_{1g} skeletal modes of the porphyrin. The non-totally symmetric (mainly B_{1g}) modes have been resolved only poorly, because of the lack of resonance enhancement in the violet range of wavelengths. From Fig. 3 and Table 1, it follows that the non-totally symmetric skeletal modes of Zn-OEP (A_{2g} and B_{1g}/B_{2g} symmetry) are resonance enhanced in the present CARS configuration. Such a pattern of mode-selective resonance enhancement is consistent with that typically reported for metallo-octaethylporphyrins, which are excited in the Q_{00}–Q_{01} absorption range.[5,7,9,18,19,21,23] The most pronounced enhancement is undergone by the antisymmetric A_{2g} modes (ν_{19}, ν_{21} and ν_{22}), which are seen to dominate all spectra except spectrum (d) in Fig. 3.

In addition to the bands due to in-plane porphyrin skeletal modes, there is a pair of weaker bands (such as those at 1267 and 1320 cm^{-1}) which are attributable to the ethyl substituents.[9] According to the porphyrin force field analysis,[9] local modes of ethyl groups can be assigned to A_1, B_1/B_2 or A_2 symmetry. Neither of the two ethyl modes resolved in the CARS spectra displays an unmixed polarization character, which would be associated with a ratio ρ^R of either 0.125 or 0.75 or $-\infty$. It is therefore possible that the depolarization ratios of ethyl modes in Table 1 characterize the envelopes of overlapping vibrations of the same origin (e.g. CH_2 twisting or wagging), but of various symmetry groups. This is supported by resonance Raman spectra, where these modes show a selective enhancement at different wavelengths.[3,7–9] A weak band at 1368 cm^{-1}, that appears as a negative peak in spectrum (a) in Fig. 3, is clearly of antisymmetric character ($\rho^R = -0.97$). An anomalously polarized band at this wavenumber has previously been observed in the Q-band range excited Ni-OEP[7,9] and is probably due to in-phase methyl group deformations.

Table 1. The best parameter sets as obtained from a global fit on the seven polarized multiplex CARS spectra of Zn-OEP in toluene[a]

$\frac{\Omega_t}{2\pi c}$/cm^{-1}	$\frac{\Gamma_t}{2\pi c}$/cm^{-1}	A_t^R/au	Θ_t^R/°	ρ_t^R	Assignment
1367.9	9.0	1.4	−88	−0.97	Methyl, CH_3 in-phase def.
1318.1	10.7	3.7	86	0.21	Ethyl, CH_2 wag.
1266.7	12.4	1.3	−64	0.59	Ethyl, CH_2 twist
1560.4	15.8	1.8	−104	−9.2	A_{2g}, ν_{19}
1390.9	10.7	1.3	−96	−4.8	A_{2g}, ν_{20}
1320.3	9.4	2.0	−108	−11.4	A_{2g}, ν_{21}
1140.8	8.1	1.0	−119	−5.0	A_{2g}, ν_{22}
1468.0	12.1	1.0	87	0.74	B_{2g}, ν_{28}
1409.0	11.9	6.0	121	0.76	B_{2g}, ν_{29}
1618.3	12.7	13.6	97	0.73	B_{1g}, ν_{10}
1559.5	12.6	15.5	103	0.75	B_{1g}, ν_{11}
1212.1	11.1	9.2	116	0.73	B_{1g}, ν_{13}

[a] The parameters include the Raman band positions, bandwidths, relative amplitudes, coherent phases and depolarization ratios. Modes are labelled according to the literature.[2,5,6,9,18,21] Fitting parameters for the non-resonant background are χ^{NR} = 63 au and $\rho^{NR} = 0.3283$.

Reconstruction of polarized Raman spectra

Although it is not possible to measure the spontaneous Raman (SR) spectra of Zn-OEP in the Q-band region, the CARS spectra can be used to reconstruct the spontaneous Raman spectra. However, as a result of the interference between closely spaced vibrations and a further interference with the non-resonant background, the polarized *coherent* Raman spectra are more complicated than those of *spontaneous* Raman (SR) scattering. It is therefore useful to explain how a reconstruction can be done.

A formal difference between coherent (frequency-degenerate CARS, ρ^R) and spontaneous (ρ_{SR}) depolarization ratios is that the former is defined as a ratio of susceptibility tensor components, whereas the latter is defined as a ratio of scattering intensities:

$$\rho^R \equiv \chi^{(3)R}_{1221} \Big/ \chi^{(3)R}_{1111} \quad \text{and} \quad \rho_{SR} \equiv I^{SR}_{\perp} \Big/ I^{SR} \tag{5}$$

Each ratio can also be expressed in terms of the invariants of the scattering tensor [susceptibility $\chi^{(3)R}$ or Raman polarizability $\tilde{\alpha}$, respectively]:[17,25]

$$\rho^R = \frac{-5\overline{\gamma_A^2} + 3\overline{\gamma^2}}{45\overline{\alpha^2} + 4\overline{\gamma^2}} \quad \text{and} \quad \rho_{SR} = \frac{5\overline{g_A^2} + 3\overline{g^2}}{45\overline{a^2} + 4\overline{g^2}} \tag{6}$$

Whereas the SR ratio ρ_{SR} is always a real positive number, the CARS ratio ρ^R may well be complex. The complexity occurs in the range of optical absorption, since the coherent invariants $\overline{\alpha^2}$, $\overline{\gamma^2}$ and $\overline{\gamma_A^2}$, in general all have different vibronic resonances and hence have different phases.

For a vibration of an optically transparent medium with a non-degenerate ground state, neither the susceptibility tensor $\chi^{(3)R}$ nor the polarizability tensor α can have an antisymmetric component. Therefore, the invariants $\overline{\gamma_A^2}$ and $\overline{g_A^2}$ vanish. The remaining coherent invariants $\overline{\alpha^2}$ (isotropy) and $\overline{\gamma^2}$ (anisotropy) are then essentially real numbers, and can be related to their spontaneous counterparts ($\overline{\alpha^2} \rightarrow \overline{a^2}$ and $\overline{\gamma^2} \rightarrow \overline{g^2}$). The ratios ρ_{SR} and ρ^R are then equal and they vary between 0 ($\overline{\gamma^2}, \overline{g^2} = 0$) and 0.75 ($\overline{\alpha^2}, \overline{a^2} = 0$). The reconstruction of polarized SR spectra of a transparent compound can be carried out using the values of vibrational frequencies Ω_t, bandwidths Γ_t, amplitudes A_t^R and depolarization ratios ρ_t^R derived from the CARS fit:

$$I_{\parallel}^{SR}(\omega) \propto \sum_t A_t^R L(\Omega_t - \omega, \Gamma_t) \quad \text{and}$$

$$I_{\perp}^{SR}(\omega) \propto \sum_t \rho_t^R A_t^R L(\Omega_t - \omega, \Gamma_t) \qquad (7)$$

with ω being the Stokes shift and $L(\Omega_t - \omega, \Gamma_t)$ being a normalized lineshape function (most typically a Lorentzian).

The validity of the above considerations was verified by comparing the reconstructed spontaneous Raman spectra of toluene with the experimental spontaneous Raman spectrum [Fig. 4(A)]. The agreement is very good and also serves to show that the CARS fitting procedure is reliable.

In some cases Eqns (7) are also applicable in simulating Raman spectra of compounds in resonant excitation. For a vibration of either exact A_{1g} symmetry ($\overline{\gamma_A^2} = 0$) or exact B_{1g}/B_{2g} symmetry ($\overline{\alpha^2}, \overline{\gamma_A^2} = 0$), the two susceptibility components $\chi_{1111}^{(3)R}$ and $\chi_{1221}^{(3)R}$ are always in-phase. Hence even in a range of electronic absorption the resultant coherent ratios ρ^R can be treated as real values, yielding the following relations: $\rho^R = \rho_{SR} = 0.125$ (A_{1g} mode) and $\rho^R = \rho_{SR} = 0.75$ (B_{1g}/B_{2g} mode). For a mode of exact A_{2g} symmetry only the antisymmetric invariant (γ_A) remains non-zero ($\overline{\alpha^2}, \overline{\gamma^2} = 0$), and thus $\rho^R = -\rho_{SR} = -\infty$ [the complexity of ρ^R being fully contained in the coherent vibrational phase, that is only retrievable from the $\chi_{1221}^{(3)R}$ spectra].

From Table 1 it can be observed that the values of coherent ratios ρ^R displayed by the Zn-OEP skeletal modes are characteristic of the exact B_{1g}/B_{2g} or A_{2g} vibrational symmetries. While this indicates inactivity of symmetry lowering distortions[7] within D_{4h} effective symmetry of Zn-OEP,[2] it is more important that the mode symmetries are unmixed and the coherent invariants can be separated. Thus, in order to reconstruct a pair of polarized SR spectra of Zn-OEP using the CARS-fit vibrational parameters, it is sufficient to (i) omit the coherent phases Θ_t^R, (ii) invert the negative sign of coherent ratios ρ^R for A_{2g} modes and (iii) make use of Eqns (7). Polarized SR spectra [Fig. 4(B)] of Zn-OEP are thus reconstructed using the CARS fit parameters from Table 1.

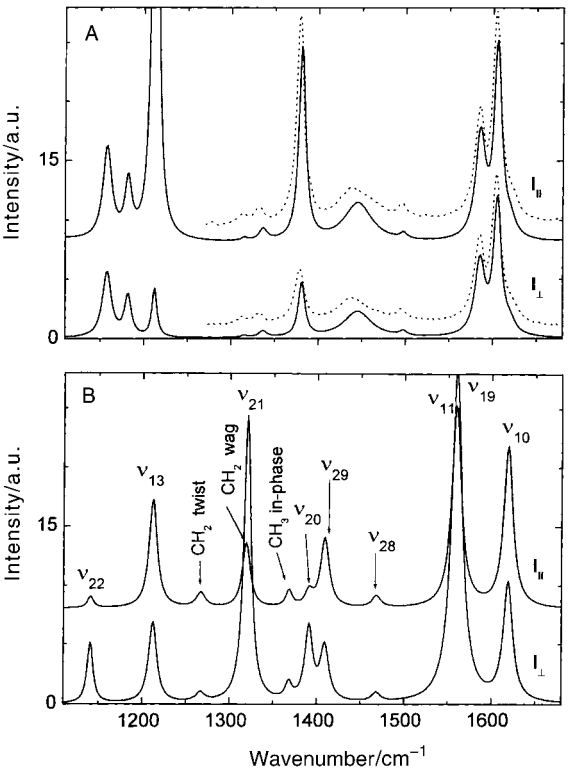

Figure 4. (A) Polarized spontaneous Raman spectra of neat toluene reconstructed with parameters obtained from CARS fit (solid lines). The spontaneous Raman spectra (dotted lines) are shifted upwards to allow a comparison. (B) Polarized Raman spectra of Zn-OEP (only porphyrin vibrations considered) reconstructed from the set of CARS fitting parameters in Table 1. A Lorentzian line function is assumed for all vibrations.

Coherent vibrational phase of porphyrin modes

Figure 5 summarizes the information on coherent vibrational phases of Zn-OEP skeletal modes as obtained from CARS spectral analysis. The values of the coherent phases are similar for vibrational bands with the same symmetry. The similarity in phases of the B_{1g} and B_{2g} modes is not surprising, since the only distinction between the two symmetries is the choice of the molecular frame. It is remarkable that the phases of the Zn-OEP modes exhibit such a clear correlation with the mode polarization character.

A similar correlation has also been observed in copper(II)-tetraphenylporphyrin (Cu-TPP) excited in the Q-band absorption range.[22] The correlation can be understood using the Herzberg–Teller expansion of the molecular polarizability.[22] We carried out an analogous analysis for the modes of Zn-OEP. The procedure contains the following steps: (i) the parameters (electronic frequencies, bandwidths, dipole amplitudes, potential energy displacements and the vibronic couplings) that describe the porphyrin electronic

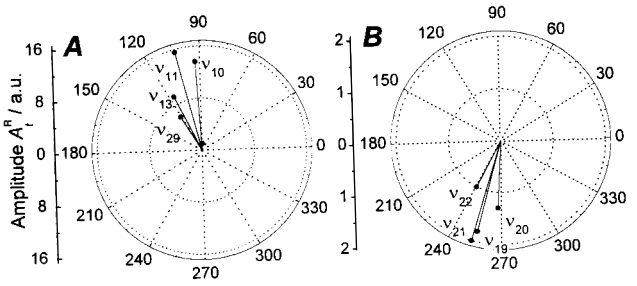

Figure 5. Phase diagrams showing coherent vibrational amplitudes A_t^R and phases Θ_t^R of (A) depolarized vibrations with either B_{1g} or B_{2g} symmetry and (B) anomalously polarised (A_{2g} symmetry) skeletal modes of Zn-OEP from Table 1. The arbitrariness in the determination of the phase values is $\pm 360°$.

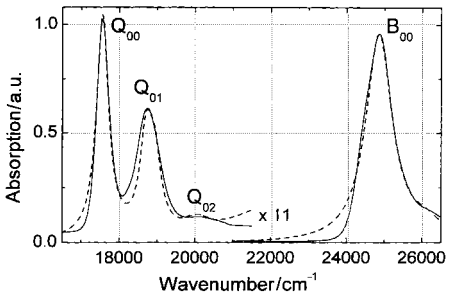

Figure 6. Absorption spectrum of Zn-OEP in toluene (solid line) compared with the calculated profile (dashed line) that results from simulations taking into account three vibrational modes ν_{13} (1212 cm^{-1}), ν_{29} (1409 cm^{-1}) and ν_{21} (1320 cm^{-1}). The parameters of these modes are listed in Table 2. The absorption in the Q band range is magnified.

structure were obtained from the fit of Zn-OEP absorption spectrum according to Eqns (6)–(9) in Ref. 22 and (ii) a true multimode description is replaced by a more manageable three-mode approximation. The absorption spectrum of Zn-OEP was simulated, following Gouterman's four-orbital model,[4] considering the vibronic activity of three porphyrin modes with different polarization character, namely of B_{1g} (ν_{13} at 1212 cm^{-1}), B_{2g} (ν_{29} at 1409 cm^{-1}) and A_{2g} (ν_{21} at 1320 cm^{-1}). Figure 6 shows a comparison of the actual absorption spectrum of Zn-OEP with the simulated profile. The fitting parameters are listed in Table 2. Reasonable agreement between the two curves is obtained. Particularly the shape of the absorption band in the Q_{00} band range, where the current CARS spectra were acquired, is well reproduced by the simulated profile. A discrepancy remaining at ca 22 000–24 000 cm^{-1} is due to the asymmetric shape of the inhomogeneously broadened B band, which cannot be reproduced using the assumed Lorentzian line shape function. This approach nevertheless results in reasonable numbers for the frequencies Ω_{k0} and bandwidths of the porphyrin electronic transitions for which the coherent vibrational phases are most sensitive.

Obviously, the three-mode model utilized is too simple to describe the complete optical response and hence the vibronic structure of Zn-OEP. However, it does allow the prediction of the dispersion of the coherent phase versus the excitation frequency that is *characteristic* for the mode of a particular vibrational symmetry.

As follows from the discussion above, the dispersion of the coherent phases of the B_{1g}/B_{2g} and A_{2g} modes is governed by the dispersion of the coherent invariants $\overline{\gamma^2}$ and γ_A^2, respectively. From Eqns (5)–(7) it follows that the phases of the susceptibility components $\chi^{(3)}_{1111}$ and $\chi^{(3)}_{1221}$ are identical for the modes of exact B_{1g}/B_{2g} symmetry and are both given by the phase of the anisotropic invariant $\overline{\gamma^2}$. Since A_{2g} modes do not contribute to the dispersion of $\chi^{(3)}_{1111}$ at all, the phase of an A_{2g} mode is that of the $\chi^{(3)}_{1221}$ component, and thus of $-\overline{\gamma_A^2}$. Figure 7 shows the dispersion of the coherent vibrational phases of B_{1g}/B_{2g} and A_{2g} modes of Zn-OEP in the Q_{00}–Q_{01} absorption range as calculated according to the theory in Ref. 22 with the parameters listed in Table 2. As one can see from Fig. 7, near the Q_{00} resonance ($\omega_1 \approx \Omega_{Q00}$) the dispersion of coherent phases becomes uniform for all modes of the same symmetry group regardless of the frequency Ω_t. The phase values that result from the model calculations are in a good agreement with those derived from the polarized CARS

Table 2. Parameter set that is used to fit the absorption spectrum of Zn-OEP, using a three-dimensional harmonic oscillator approximation[a]

State	Position	Amplitude	Width	B_{1g}, at 1212 cm^{-1}		B_{2g}, at 1409 cm^{-1}		A_{2g}, at 1320 cm^{-1}	
k	$\Omega_k/2\pi c$ cm^{-1}	R_{gk} au	$\Gamma_k/\pi c$ cm^{-1}	Δ au	$h_{jak}/\hbar$ cm^{-1}	Δ au	$h_{jak}/\hbar$ cm^{-1}	Δ au	$h_{jak}/\hbar$ cm^{-1}
Q_X	17 555	1	380	0.31	h_{BB1gQ} =	0.29	h_{BB2gQ} =	0	h_{BA2gQ} =
Q_Y	17 555	1	380	−0.31	1600	−0.29	1200	0	1500
B_X	24 850	3.15	850	0.31	h_{QB1gB} =	0.29	h_{QB2gB} =	0	h_{QA2gB} =
B_Y	24 850	3.15	850	−0.31	1600	−0.29	1200	0	1500

[a] The electronic transition is indicated by k (first column); the frequency position of the top, the amplitude and the bandwidth of the electronic transition are presented in columns 2, 3 and 4, respectively. The next three pairs of columns present the shift of the excited-state potential with respect to the ground state along the nuclear coordinate (first column in each pair) and the magnitude of the vibronic coupling operator h_{jak} (second column of each pair) for each of the three-harmonic oscillator.

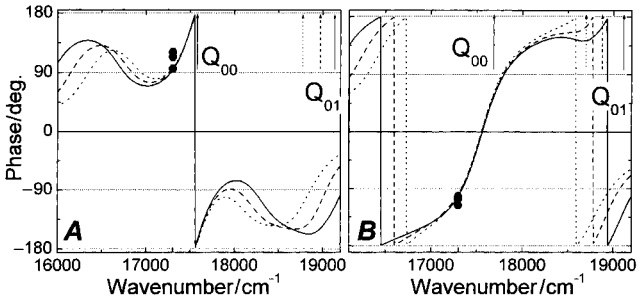

Figure 7. (A) The calculated dispersion curve of the phase arguments of $\chi^{(3)}_{1111}(\omega_{CARS};\omega_1,\omega_1,-\omega_2)$ for three different B_{1g}/B_{2g} modes of Zn-OEP versus excitation frequency ω_1 in the Q band range. Solid line, ν_{10} (1618 cm^{-1}); dashed line, ν_{29} (1409 cm^{-1}); dotted line, ν_{13} (1212 cm^{-1}). (B) The calculated dispersion curve of the phase arguments of $\chi^{(3)}_{1221}(\omega_{CARS};\omega_1,\omega_1,-\omega_2)$ for three different antisymmetric A_{2g} modes. The curves are calculated with $\omega_2=\omega_1-\Omega_t$ and $\omega_{CARS}=\omega_1+\Omega_t$, Ω_t being the frequency of *t*th mode of Zn-OEP, as derived from the CARS lineshape fit. Solid line, ν_{19} (1560 cm^{-1}); dashed line, ν_{21} (1320 cm^{-1}); dotted line, ν_{22} (1140 cm^{-1}). The experimental phase values (filled markers) result from the CARS fit (Table 1) at $\omega_1/2\pi c = 17\,240$ cm^{-1}. The arrows denote the positions of 0–0 and the 0–1 absorption maxima.

experiment (filled symbols in Fig. 7) at $\omega_1/2\pi c = 17\,240$ cm^{-1}. This corroborates a similar correlation obtained earlier for the coherent phase behaviour in CARS spectra of Cu-TPP.

CONCLUSIONS

We have reported the vibrational bands of the highly luminescent compound Zn-OEP. This was possible using the polarization-sensitive MCARS technique. Quantitative results were obtained from a global fit of the seven polarized CARS spectra to the expression for the CARS dispersion equation. The CARS spectra of Zn-OEP, obtained with Q-band excitation, are dominated by B_{1g}, B_{2g} and A_{2g} skeletal modes of the porphyrin macrocycle. The mode classification and the assignment were made on the basis of the coherent depolarization ratios which were obtained directly from the fit together with the band positions, bandwidths, amplitudes and phases. The parameter set for the solvent allows a precise reconstruction of the polarized spontaneous Raman spectra. A similar reconstruction of the spontaneous Raman spectrum on the basis of the CARS spectrum of Zn-OEP gives a prediction of the spontaneous Raman spectrum.

The correlation between the magnitude of coherent vibrational phase exhibited by B_{1g}/B_{2g} and A_{2g} modes of Zn-OEP and the mode symmetry confirms a similar correlation obtained in case of Cu-TPP.[22] In the latter case the macroscopic susceptibility $\chi^{(3)}$ was described in terms of a multi-dimensional set of harmonic oscillators in the Herzberg–Teller expansion of the molecular polarizability. Application of that model to the results obtained for Zn-OEP corresponds well and gives further support for the theoretical approach in Ref. 22.

The introduction of a head-to-head arrangement of microscope objectives in the CARS spectrometer leads to several advantages: (i) reduction of the amount and the costs of sample used, (ii) acquisition of panoramic (ca 600 cm^{-1} broad) CARS spectra with no need for pump wavelength readjustment and (iii) increase in the incident intensities, which is particularly of importance for the broadband Stokes beam. This arrangement makes it relatively simple to obtain high-quality CARS spectra of dilute systems in the condensed phase.

Acknowledgements

S. G. Kruglik, gratefully acknowledges receipt of a grant from the Netherlands Organization for Scientific Research (NWO) and support from the Stichting Universiteitsfonds Twente.

REFERENCES

1. Kumble R, Hu S, Loppnow GB, Vitols SE, Spiro TG. *J. Phys. Chem.* 1993; **97**: 10521.
2. Kumble R, Loppnow GB, Hu S, Mukherjee A, Thompson MA, Spiro TG. *J. Phys. Chem.* 1995; **99**: 5809.
3. Kreszowski DH, Deinum G, Babcock GT. *J. Am. Chem. Soc.* 1994; **116**: 7463.
4. Gouterman M. *J. Chem. Phys.* 1959; **30**: 1139; Gouterman J. In *The Porphyrins*, vol. 3, Dolphin D (ed.). Academic Press: New York, 1978, Chapt. 1, 1.
5. Abe M, Kitagawa T, Kuogoku Y. *J. Chem. Phys.* 1978; **69**: 4526.
6. Zgierski MZ, Pawlikowski M. *Chem. Phys.* 1982; **65**: 335.
7. Bobinger U, Schweitzer-Stenner R, Dreybrodt W. *J. Phys. Chem.* 1991; **95**: 7625.
8. Spaulding LD, Chang CC, Yu N.-T, Felton RH. *J. Am. Chem. Soc.* 1975; **97**: 2517.
9. Li X-Y, Czernuszewicz RS, Kincaid JR, Stein P, Spiro TG. *J. Phys. Chem.* 1990; **94**: 47.
10. Sato S, Kitagawa T. *Appl. Phys. B* 1994; **59**: 415.
11. Rodrigues J, Kirmaier C, Holten D. *J. Am. Chem. Soc.* 1989; **1111**: 6500.
12. Akhmanov SA, Bunkin AF, Ivanov SG, Koroteev NI, *Sov. Phys. JETP* 1978 **47**, 667.
13. Oudar J-L, Smith RW, Shen YR. *Appl. Phys. Lett.* 1979; **34**: 758.
14. Voroshilov A, Lucassen GW, Otto C, Greve J. *J. Raman Spectrosc.* 1995; **26**: 443.
15. Voroshilov A, Otto C, Greve J. *Appl. Spectrosc.* 1996; **50**: 78.
16. Nestor JR. *J. Raman Spectrosc.* 1978; **7**: 90.
17. Igarashi R, Adachi Y, Maeda S. *J. Chem. Phys.* 1980; **72**: 4308.
18. Apanasevich PA, Kvach VV, Orlovich VA. *J. Raman Spectrosc.* 1989; **20**: 125.
19. Kamalov VF, Koroteev NI, Toleutaev BN. In *Time Resolved Spectroscopy*, Clark RJH, Hester RW (eds). Wiley: New York, 1989; Chapt. 6, 255–299.
20. Lucassen GW, de Boeij WP, Greve J. *J. Raman Spectrosc.* 1993; **24**: 383.
21. Kruglik SG, Apanasevich PA, Chirvony VA, Kvach VV, Orlovich VA. *J. Phys. Chem.* 1995; **99**: 2978.
22. Voroshilov A, Otto C, Greve J. *J. Chem. Phys.* 1997; **106**: 2589.
23. Nissum M, Funk J-M, Kiefer W. *J. Raman Spectrosc.* 1999; **30**: 605.
24. Bjorklund GC. *IEEE J. Quantum Electron.* 1975; **11**: 287.
25. Johnson BB, Peticolas WL. *Annu. Rev. Phys. Chem.* 1976; **27**: 465.